PHYSICAL REVIEW D **83,** 094506 (2011)

Aoki phases in the lattice Gross-Neveu model with flavored mass terms

Michael Creutz*
Physics Department, Brookhaven National Laboratory, Upton, New York 11973, USA

Taro Kimura†
Department of Basic Science, University of Tokyo, Tokyo 153-8902, Japan

Tatsuhiro Misumi‡
Yukawa Institute for Theoretical Physics, Kyoto University, Kyoto 606-8502, Japan
(Received 8 March 2011; published 23 May 2011)

We investigate the parity-broken phase structure for staggered and naive fermions in the Gross-Neveu model as a toy model of QCD. We consider a generalized staggered Gross-Neveu model including two types of four-point interactions. We use generalized mass terms to split the doublers for both staggered and naive fermions. The phase boundaries derived from the gap equations show that the mass splitting of tastes results in an Aoki phase both in the staggered and naive cases. We also discuss the continuum limit of these models and explore taking the chirally symmetric limit by fine-tuning a mass parameter and two-coupling constants. This supports the idea that in lattice QCD we can derive one- or two-flavor staggered fermions by tuning the mass parameter, which are likely to be less expensive than Wilson fermions in QCD simulation.

DOI: 10.1103/PhysRevD.83.094506 PACS numbers: 11.15.Ha, 11.10.Kk, 11.15.Pg, 11.30.Rd

I. INTRODUCTION

Since the pioneering work in Ref. [1], the rich phase structure in the lattice Wilson fermion has been extensively studied [2–6]. As is well known [7], Wilson fermions bypass the no-go theorem [8] and produce a single fermionic degree of freedom by breaking the chiral symmetry explicitly. This leads to an additive mass renormalization and requires fine-tuning of a mass parameter for a chiral limit. Furthermore at finite lattice spacing, there emerges a parity-broken phase (Aoki phase) [1]. The full phase diagram reflects the masses possessed by each of the original doublers. As seen from this fact, the main reason for the emergence of the parity-broken phase is that the Wilson term gives a species(taste)-sensitive mass to produce a mass splitting of species as well as breaking the chiral symmetry. The understanding of the parity-broken phase structure is not only useful for simulations with Wilson fermions, but also gives practical information for the application of overlap [9,10] and domain-wall [11,12] fermions, both of which are built on the Wilson fermion kernel. Indeed it is shown in [13] that the domain-wall fermion also possesses a complicated parity-broken phase diagram for a finite size of the extra dimension.

On the other hand, no parity-broken phase structure is observed in staggered fermions [14–16] with their exact chiral symmetry. However things could be changed if we introduce a taste-sensitive mass term, which we refer to as a taste splitting or flavored mass in this paper. Adams recently established theoretical foundation of the index theorem with staggered fermions [17] and presented a new version of the overlap fermion constructed from the staggered kernel [18,19]. He introduced a taste-splitting mass term for the spectral flow to detect the index correctly. This mass term assigns positive and negative masses to tastes depending on their flavor chiralities. After these works the present authors [20] successfully defined the index in the naive and minimally doubled fermions [21–24] and presented new versions of overlap fermions by implementing the flavored mass terms [25]. It is natural to consider the phase diagram for these fermions with the mass splitting of the tastes since it is also useful for the practical application of their overlap versions as well as themselves.

In this paper we study the parity-broken phase structure for naive and staggered fermions with the flavored mass terms. We use the two-dimensional lattice Gross-Neveu models [3,26–30] as toy models of QCD. We develop the generalized staggered Gross-Neveu model including two types of four-point interactions to study the staggered phase structure. We solve the gap equations for the large N limit and obtain the phase boundaries in the M-g^2 plane. We show the Aoki phase exists both in staggered and naive cases reflecting the mass splitting of tastes. In the naive cases there are varieties of the phase diagram depending on linear combinations of two types of the flavored masses. This elucidation of the phase structure can contribute to the practical application of these fermions and their overlap versions. We also discuss the continuum limits of these Gross-Neveu models. We show that we can take the chiral continuum limit with the associated number of massless

*creutz@bnl.gov
†kimura@dice.c.u-tokyo.ac.jp
‡misumi@yukawa.kyoto-u.ac.jp

fermions by fine-tuning a mass parameter and two-coupling constants. It indicates that, in Lattice QCD with the staggered fermions with the Adams-type [18] or Hoelbling-type [19] flavored masses, we can obtain the two- or one-flavor massless fermions in the chiral and continuum limit by tuning the mass parameter. They can be less expensive than Wilson fermions in lattice QCD simulations.

In Sec. II we study the parity-broken phase diagram by using the naive Gross-Neveu model with the flavored mass. In Sec. III we propose the generalized staggered Gross-Neveu model and study the phase diagram. In Sec. IV we investigate the continuum limit of these models and discuss the first order phase boundaries in the phase diagram. Section V is devoted to a summary and discussion.

II. NAIVE GROSS-NEVEU MODEL

In this section we investigate the phase diagram for naive lattice fermions with flavored mass terms by using the $d = 2$ Gross-Neveu model, which has lots of common features with QCD. Let us begin with the lattice Gross-Neveu model with the flavored mass term, which is given by

$$S = \frac{1}{2}\sum_{n,\mu}\bar{\psi}_n\gamma_\mu(\psi_{n+\mu} - \psi_{n-\mu}) - \frac{g^2}{2N}\sum_n[(\bar{\psi}_n\psi_n)^2 + (\bar{\psi}_n i\gamma_5\psi_n)^2] + \sum_{n,m}\bar{\psi}_n(M\delta_{nm} + (M_f)_{n,m})\psi_m, \quad (1)$$

where μ stands for $\mu = 1, 2$, $n = (n_1, n_2)$ are the two-dimensional coordinates and ψ_n stands for a N-component Dirac fermion field $(\psi_n)_j (j = 1, 2, \ldots, N)$. We note the bilinear $\bar{\psi}\psi$ means $\sum_{j=1}^N \bar{\psi}_j\psi_j$. g^2 corresponds to the 't Hooft coupling. M is a usual mass assigning the same mass to species while $(M_f)_{n,m}$ is a flavored mass assigning different masses to them. Here we define the two-dimensional gamma matrices as $\gamma_1 = \sigma_1$, $\gamma_2 = \sigma_2$ and $\gamma_5 = \sigma_3$. We make all the quantities dimensionless in this equation. Here we consider scalar and pseudoscalar four-fermi interactions which are sufficient to study the parity-phase structure. By introducing auxiliary bosonic fields σ_n, π_n we remove the four-point interactions as

$$S = \frac{1}{2}\sum_{n,\mu}\bar{\psi}_n\gamma_\mu(\psi_{n+\mu} - \psi_{n-\mu}) + \sum_{n,m}\bar{\psi}_n(M_f)_{n,m}\psi_m + \frac{N}{2g^2}\sum_n((\sigma_n - M)^2 + \pi_n^2) + \sum_n\bar{\psi}_n(\sigma_n + i\gamma_5\pi_n)\psi_n. \quad (2)$$

By solving the equations of motion, we show the following relation between these auxiliary fields and the bilinears of the fermion fields

$$\sigma_n = M - \frac{g^2}{N}\bar{\psi}\psi, \quad (3)$$

$$\pi_n = -\frac{g^2}{N}\bar{\psi}i\gamma_5\psi. \quad (4)$$

These relations indicate how σ and π stand for the scalar and pseudoscalar mesons. After integrating the fermion fields, the partition function and the effective action with these auxiliary fields are given by

$$Z = \int\prod_n(d\sigma_n d\pi_n)e^{-NS_{\rm eff}(\sigma,\pi)}, \quad (5)$$

$$S_{\rm eff}(\sigma_n, \pi_n) = \frac{1}{2g^2}\sum_n((\sigma_n - M)^2 + \pi_n^2) - {\rm Tr}\log D_{n,m}, \quad (6)$$

with

$$D_{n,m} = (\sigma_n + i\gamma_5\pi_n)\delta_{n.m} + \frac{\gamma_\mu}{2}(\delta_{n+\mu,m} - \delta_{n-\mu,m}) + (M_f)_{n,m}. \quad (7)$$

Here Tr stands for the trace both for the position and spinor spaces. As is well known, the partition function in the Gross-Neveu model is given by the saddle point of this effective action in the large N limit. We denote as $\tilde{\sigma}_n$, $\tilde{\pi}_n$ solutions satisfying the saddle-point conditions

$$\frac{\delta S_{\rm eff}(\sigma_n, \pi_n)}{\delta\sigma_n} = \frac{\delta S_{\rm eff}(\sigma_n, \pi_n)}{\delta\pi_n} = 0. \quad (8)$$

Then the partition function is given by

$$Z = e^{-S_{\rm eff}(\tilde{\sigma},\tilde{\pi})}. \quad (9)$$

By assuming the translational invariance we define the position-independent solutions as $\sigma_0 \equiv \tilde{\sigma}_0$ and $\pi_0 \equiv \tilde{\pi}_0$ Then we can factorize a volume factor $V = \sum_n 1$ in the effective action as

$$S_{\rm eff} = V\tilde{S}_{\rm eff}(\sigma_0, \pi_0), \quad (10)$$

$$\tilde{S}_{\rm eff}(\sigma_0, \pi_0) = \frac{1}{2g^2}((\sigma_0 - M)^2 + \pi_0^2) - \frac{1}{V}{\rm Tr}\log D. \quad (11)$$

We can write ${\rm Tr}\log D$ in a simple form by the Fourier transformation to momentum space

$${\rm Tr}\log D = V\int\frac{d^2k}{(2\pi)^2}\log\Big[\det\Big(\sigma_0 + i\gamma_5\pi_0 + M_f(k) + i\sum_\mu\gamma_\mu\sin k_\mu\Big)\Big] = V\int\frac{d^2k}{(2\pi)^2}\log[(\sigma_0 + M_f(k))^2 + \pi_0^2 + s^2], \quad (12)$$

with det being the determinant in the spinor space and $s^2 = \sum_\mu \sin^2 k_\mu$. $M_f(k)$ is the flavored mass represented in momentum space. Now the saddle-point equations are written as

$$\frac{\delta \tilde{S}_{\rm eff}}{\delta \sigma_0} = \frac{(\sigma_0 - M)}{g^2} - 2\int \frac{d^2k}{(2\pi)^2} \frac{\sigma_0 + M_f(k)}{(\sigma_0 + M_f(k))^2 + \pi_0^2 + s^2} = 0, \quad (13)$$

$$\frac{\delta \tilde{S}_{\rm eff}}{\delta \pi_0} = \frac{\pi_0}{g^2} - 2\int \frac{d^2k}{(2\pi)^2} \frac{\pi_0}{(\sigma_0 + M_f(k))^2 + \pi_0^2 + s^2} = 0. \quad (14)$$

In this section we consider two types of the flavored mass for the naive fermion

$$M_f^{(1)}(k) = \cos k_1 \cos k_2, \quad (15)$$

$$M_f^{(2)}(k) = \tfrac{1}{2}(\cos k_1 + \cos k_2)(1 + \cos k_1 \cos k_2). \quad (16)$$

Such mass terms were first introduced in the minimally doubled fermion by using the point-splitting method [25]. Then these were introduced also for the naive fermion to consider the index theorem and a new type of overlap fermions [20]. Studying the phase diagram with these flavored mass terms not only contributes to understanding the overlap versions but also helps to understand the staggered case in the next section. Here σ_0 and π_0 are determined as $\sigma_0(M, g^2)$, $\pi_0(M, g^2)$ from the saddle-point equations once the values of M and g^2 are fixed.

Let us look into the phase structure with respect to parity symmetry. The order parameter of this symmetry is π_0, which can take zero or nonzero values depending on values of M and g^2. Parity symmetry is spontaneously broken for the nonzero cases $\pi_0 \neq 0$. The phase boundary is determined by imposing $\pi_0 = 0$ on Eqs. (13) and (14) after the overall π_0 being removed in Eq. (14). Then the conditions for the phase boundary, so-called gap equations, are given by

$$\frac{M_c}{g^2} = -2\int \frac{d^2k}{(2\pi)^2} \frac{M_f(k)}{(\sigma_0 + M_f(k))^2 + s^2}, \quad (17)$$

$$\frac{1}{g^2} = 2\int \frac{d^2k}{(2\pi)^2} \frac{1}{(\sigma_0 + M_f(k))^2 + s^2}, \quad (18)$$

with M_c being the critical value of M. As we will check later, this phase boundary is a second-order critical line. Here we derive the parity-phase boundary $M_c(g^2)$ as a function of the coupling g^2 by getting rid of the chiral condensate σ_0 from these equations. We will calculate the parity-phase boundaries for three cases of the flavored masses $M_f^{(1)}$, $M_f^{(2)}$ and $M_f^{(1)} + M_f^{(2)}$.

A. $M_f^{(1)}$

The lattice fermion action with this flavored mass assigns the positive mass $m = 1$ to two species with the momentum $(0, 0)(\pi, \pi)$ and the negative mass $m = -1$ to the other two species with $(0, \pi)(\pi, 0)$. Before calculating $M_c(g^2)$ numerically, we can anticipate the phase structure from the symmetry of the gap equations. To see this we replace k_1 by $\pi - k_1$ in (13) and (14) for $M_f^{(1)}$. Then the equations are converted into

$$\frac{-\sigma_0 + M}{g^2} = 2\int \frac{d^2k}{(2\pi)^2} \frac{-\sigma_0 + M_f^{(1)}(k)}{(-\sigma_0 + M_f^{(1)}(k))^2 + \pi_0^2 + s^2}, \quad (19)$$

$$\frac{\pi_0}{g^2} = 2\int \frac{d^2k}{(2\pi)^2} \frac{\pi_0}{(-\sigma_0 + M_f^{(1)}(k))^2 + \pi_0^2 + s^2}. \quad (20)$$

Thus, if (σ_0, π_0) are solutions for (M, g^2), $(-\sigma_0, \pi_0)$ are solutions for $(-M, g^2)$. It also means, if (M_c, g^2) is a critical point, $(-M_c, g^2)$ too. We can anticipate the phase diagram for this case is symmetric about $M = 0$. Now we derive the parity-phase boundary $M_c(g^2)$ numerically for $M_f^{(1)}(k) = \cos k_1 \cos k_2$. The phase diagram for this case is depicted in Fig. 1. A stands for the parity-symmetric phase $\pi_0 = 0$ and B for Aoki phase $\pi_0 \neq 0$. The result of the phase diagram is depicted in Fig. 2. In the large coupling

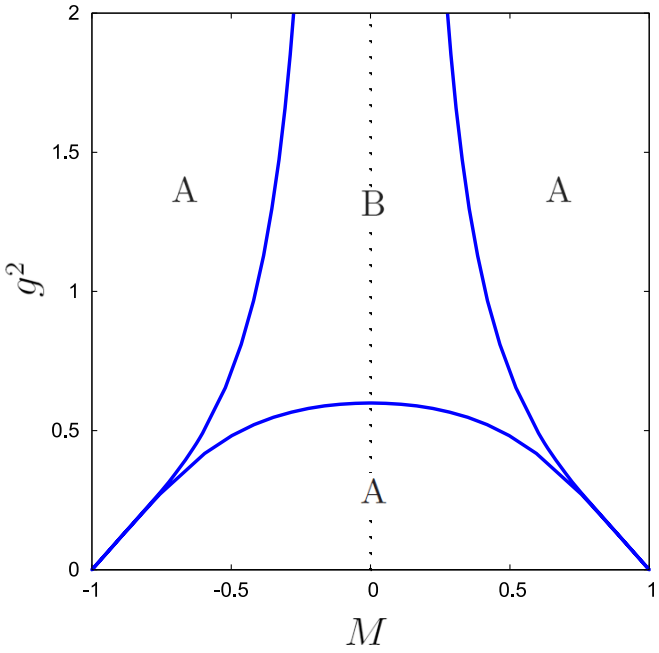

FIG. 1 (color online). Aoki phase structure for the naive fermion with the flavored mass $M_f^{(1)}$. The left and right cusps are related to two species $(0, 0)(\pi, \pi)$ with $m = 1$ and the other two $(0, \pi)(\pi, 0)$ with $m = -1$, respectively. A and B stands for parity-symmetric and -broken phases.

region there are two phase boundaries while there are four phase boundaries in the weak coupling region. The left and right cusps correspond to two species $(0, 0)(\pi, \pi)$ with the positive mass $(m = 1)$ and the other two $(0, \pi)(\pi, 0)$ with the negative mass $(m = -1)$, respectively. It reflects the mass splitting of species given by the flavored mass $M_f^{(1)}$. Here we note we obtain the same result for $-M_f^{(1)}$ except that the species $(0, 0)(\pi, \pi)$ live at the right cusp and the other two live at the left. It means the sign of the this flavored mass is irrelevant for the spectrum of the Dirac operator or the associated Aoki phase.

B. $M_f^{(2)}$

The lattice fermion action with this flavored mass assigns the positive mass $(m = 2)$ to one of four species with the momentum $(0, 0)$, zero mass to $(0, \pi)(\pi, 0)$ and the negative mass $(m = -2)$ to (π, π). To look at the symmetry of the gap equations we replace k_μ by $\pi - k_\mu$ in (13) and (14) for $M_f^{(2)}$. Then the equations are converted into

$$\frac{-\sigma_0 + M}{g^2} = 2\int \frac{d^2k}{(2\pi)^2} \frac{-\sigma_0 + M_f^{(2)}(k)}{(-\sigma_0 + M_f^{(2)}(k))^2 + \pi_0^2 + s^2}, \tag{21}$$

$$\frac{\pi_0}{g^2} = 2\int \frac{d^2k}{(2\pi)^2} \frac{\pi_0}{(-\sigma_0 + M_f^{(2)}(k))^2 + \pi_0^2 + s^2}. \tag{22}$$

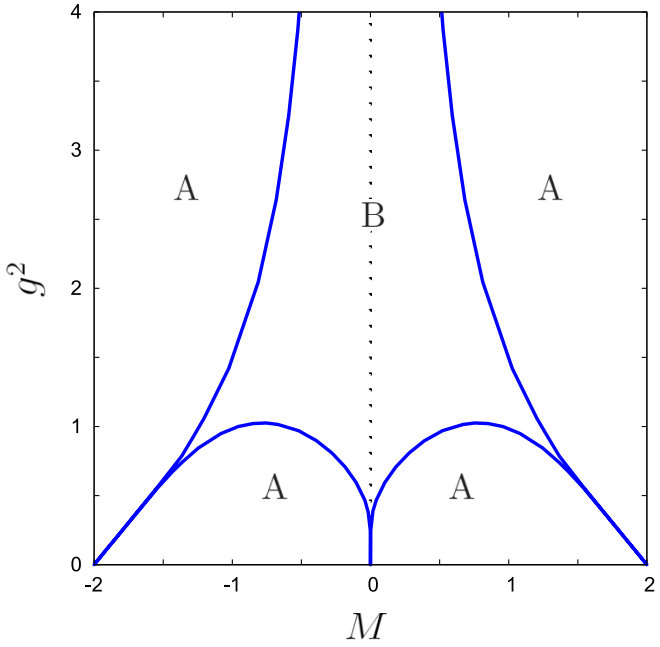

FIG. 2 (color online). Aoki phase structure for the naive fermion with the flavored mass $M_f^{(2)}$. The three cusps correspond to $(0, 0)$ with $m = 2$, $(0, \pi)(\pi, 0)$ with $m = 0$ and (π, π) with $m = -2$, respectively from the left.

Thus, if (σ_0, π_0) are solutions for (M, g^2), $(-\sigma_0, \pi_0)$ are solutions for $(-M, g^2)$. It also means, if (M_c, g^2) is a critical point, $(-M_c, g^2)$ too. We can anticipate the phase diagram for this case is again symmetric about $M = 0$. Now we derive the parity-phase boundary $M_c(g^2)$ numerically for $M_f^{(2)}(k) = (\cos k_1 + \cos k_2)(1 + \cos k_1 \cos k_2)/2$. In the large coupling region there are two phase boundaries while there are six phase boundaries in the weak coupling region. The three cusps correspond to one of four species $(0, 0)$ with $m = 2$, two of them $(0, \pi)(\pi, 0)$ with $m = 0$ and the other one (π, π) with $m = -2$, respectively from the left. It reflects the mass splitting of species given by the flavored mass $M_f^{(2)}$.

C. $M_f^{(1)} + M_f^{(2)}$

The fermion action with this flavored mass assigns the positive mass $m = 3$ to one of species with the momentum $(0, 0)$ and the negative mass $m = -1$ to the other three species with $(0, \pi)(\pi, 0)(\pi, \pi)$. Here we cannot find any relevant symmetry in the gap equations. Thus we can anticipate the phase diagram for this case is not symmetric. Now we calculate $M_c(g^2)$ numerically for $M_f^{(1)} + M_f^{(2)}(k) = \cos k_1 \cos k_2 + (\cos k_1 + \cos k_2)(1 + \cos k_1 \cos k_2)/2$. The result of the phase diagram is depicted in Fig. 3. It is obvious that it is not symmetric about $M = 0$. In the large coupling region there are two phase boundaries while there are four phase boundaries in the weak coupling region. The left and right cusps correspond to one of species $(0, 0)$ with $m = 3$ and the other three $(0, \pi)(\pi, 0)(\pi, \pi)$ with $m = -1$, respectively. It reflects the mass splitting of species given by the flavored mass

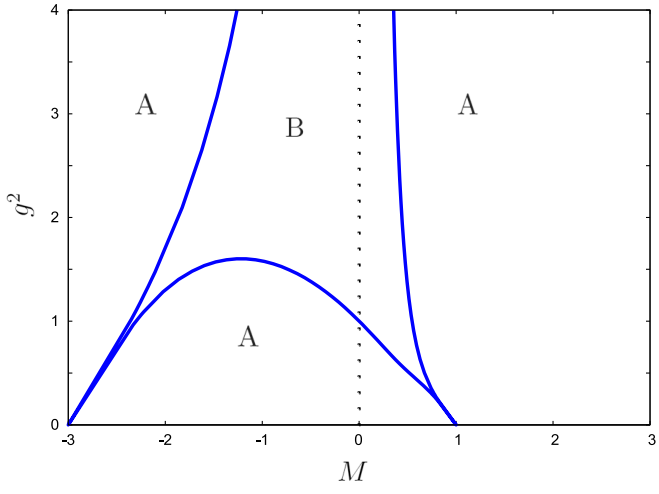

FIG. 3 (color online). Aoki phase structure for the naive fermion with the flavored mass $M_f^{(1)} + M_f^{(2)}$. The left and right cusps correspond to $(0, 0)$ with $m = 3$ and $(0, \pi)(\pi, 0)(\pi, \pi)$ with $m = -1$, respectively.

$M_f^{(1)} + M_f^{(2)}$. Now we can easily modify the phase diagram by choosing the linear combination of $M_f^{(1)}$ and $M_f^{(2)}$.

We expect these results are qualitatively similar to the phase diagram of the $d = 4$ fermion actions with the non-Abelian gauge field like QCD except for the number of species associated with each cusp. In the end of this section we check the mass of the π meson becomes zero on the critical line $M_c(g^2)$. As is well known, the correlation length gets infinitely large in the vicinity of the second and higher phase boundaries, which leads to massless dynamical degrees of freedom. In the case of lattice QCD with chiral-symmetry-broken fermions like Wilson fermion, the fine-tuning of the mass parameter to the second order phase boundary leads to the chiral limit with massless quarks and massless pions regarded as Goldstone bosons due to the spontaneous chiral symmetry breaking. Thus it is quite important to verify it. We can show the mass of π_n becomes zero on the phase boundaries as

$$\begin{aligned} m_\pi^2 &\propto \left\langle \frac{\delta^2 S_{\text{eff}}}{\delta\pi_n \delta\pi_m} \right\rangle \Big|_{M=M_c} = V \frac{\delta^2 \tilde{S}_{\text{eff}}}{\delta^2 \pi_0^2} \Big|_{M=M_c} \\ &= V\Bigg[\frac{1}{g^2} - 2\int \frac{d^2k}{(2\pi)^2} \frac{1}{(\sigma_0 + M_f(k))^2 + \pi_0^2 + s^2} - (2\pi_0^2) \\ &\quad \times \int \frac{d^2k}{(2\pi)^2} \frac{1}{((\sigma_0 + M_f(k))^2 + \pi_0^2 + s^2)^2}\Bigg]\Bigg|_{\pi_0=0} = 0. \end{aligned} \tag{23}$$

The zero mass of the pion means the phase boundary we derived is the second-order critical line. We can also check the order of the phase boundaries by depicting the potential for σ_0 and π_0 as we will discuss in Sec. IV.

III. STAGGERED GROSS-NEVEU MODEL

In this section we investigate the phase diagram for staggered fermions with the Adams-type flavored mass term by using the $d = 2$ Gross-Neveu model. To study the parity-broken phase structure we propose the generalized staggered Gross-Neveu model with the γ_5-type 4-point interaction, which is given by

$$\begin{aligned} S &= \frac{1}{2}\sum_{n,\mu} \eta_\mu \bar{\chi}_n (\chi_{n+\mu} - \chi_{n-\mu}) + \sum_n \bar{\chi}_n (M + M_f)\chi_n \\ &\quad - \frac{g^2}{2N}\sum_{\mathcal{N}}\Bigg[\Bigg(\sum_A \bar{\chi}_{2\mathcal{N}+A}\chi_{2\mathcal{N}+A}\Bigg)^2 \\ &\quad + \Bigg(\sum_A i(-1)^{A_1+A_2}\bar{\chi}_{2\mathcal{N}+A}\chi_{2\mathcal{N}+A}\Bigg)^2\Bigg], \end{aligned} \tag{24}$$

where we define two-dimensional coordinates as $n = 2\mathcal{N} + A$ with the sublattice $A = (A_1, A_2)$ $(A_{1,2} = 0, 1)$. χ_n is a one-component fermionic field. $(-1)^{A_1+A_2}$ corresponds to the natural definition of γ_5 for this fermion which is expressed as $\Gamma_{55} = \gamma_5 \otimes \gamma_5$ in the spinor-taste expression. $\eta_\mu = (-1)^{n_1+\cdots+n_{\mu-1}}$ corresponds to γ_μ. As the flavored mass term we choose the Adams-type one, which is given by

$$M_f = \Gamma_5\Gamma_{55} \sim \mathbf{1} \otimes \gamma_5 + O(a) \tag{25}$$

with the following chirality matrix Γ_5

$$\Gamma_5 = -i\eta_1\eta_2 \sum_{\text{sym}} C_1 C_2, \tag{26}$$

$$C_\mu = \tfrac{1}{2}(T_\mu + T_{-\mu}) \tag{27}$$

where T_μ is the usual translation operator. (The chirality matrix in general dimensions is defined as $\Gamma_5 \equiv -(i)^{d/2}\eta_1 \cdots \eta_d \sum_{\text{sym}} C_1 \cdots C_d$.) This mass term assigns the positive mass ($m = +1$) to one taste and the negative mass ($m = -1$) to the other depending on $\pm$ eigenvalues for $\Gamma_5\Gamma_{55}$ which we call the flavor chirality. With bosonic auxiliary fields $\sigma_{\mathcal{N}}$, $\pi_{\mathcal{N}}$, the action is rewritten as

$$\begin{aligned} S &= \frac{1}{2}\sum_{n,\mu} \eta_\mu \bar{\chi}_n (\chi_{n+\mu} - \chi_{n-\mu}) + \sum_n \bar{\chi}_n M_f \chi_n \\ &\quad + \frac{N}{2g^2}\sum_{\mathcal{N}} ((\sigma_{\mathcal{N}} - M)^2 + \pi_{\mathcal{N}}^2) \\ &\quad + \sum_{\mathcal{N},A} \bar{\chi}_{2\mathcal{N}+A}(\sigma_{\mathcal{N}} + i(-1)^{A_1+A_2}\pi_{\mathcal{N}})\chi_{2\mathcal{N}+A}, \end{aligned} \tag{28}$$

After integrating the fermion field, the partition function and the effective action with these auxiliary fields are given by

$$Z = \int (\mathcal{D}\sigma_{\mathcal{N}} \mathcal{D}\pi_{\mathcal{N}}) e^{-NS_{\text{eff}}(\sigma,\pi)}, \tag{29}$$

$$S_{\text{eff}} = \frac{1}{2g^2}\sum_{\mathcal{N}} (\sigma_{\mathcal{N}}^2 + \pi_{\mathcal{N}}^2) - \text{Tr}\log D, \tag{30}$$

with

$$\begin{aligned} D_{n,m} &= (\sigma_{\mathcal{N}} + i(-1)^{A_1+A_2}\pi_{\mathcal{N}})\delta_{n,m} \\ &\quad + \frac{\eta_\mu}{2}(\delta_{n+\mu,m} - \delta_{n-\mu,m}) + (M_f)_{n,m}. \end{aligned} \tag{31}$$

The process from (8) to (11) in the case of the naive fermion is common with this staggered case. We again denote as σ_0 and π_0 the position-independent solutions of the saddle-point equations. In this case, however, it is not straightforward to derive the $\text{Tr}\log D$ with the Dirac operator (31) in the effective action Eq. (11). In order to estimate this trace logarithm we first obtain the determinant of the Dirac operator in the sublattice space, which means the determinant in the spinor and taste spaces. Here we express the sublattice structure as a multiplet field $\tilde{\chi}_{\mathcal{N}}$ composed of the four one-component fields as

$$\tilde{\chi}_{\mathcal{N}} = \begin{pmatrix} \chi_{\rm i} \\ \chi_{\rm ii} \\ \chi_{\rm iii} \\ \chi_{\rm iv} \end{pmatrix} \tag{32}$$

where we mean $\mathrm{i} = 2\mathcal{N}$, $\mathrm{ii} = 2\mathcal{N} + (1, 0)$, $\mathrm{iii} = 2\mathcal{N} + (0, 1)$ and $\mathrm{iv} = 2\mathcal{N} + (1, 1)$. Now let us estimate the trace term

$$\mathrm{Tr}\ \log D = V \int \frac{dk^2}{(2\pi)^2} \log \det((D(k))_{ab}, \tag{33}$$

where a, b stand for the index of the four sublattices running from i to iv. Here det means the determinant with respect to the sublattice. The Dirac operator is given by

$$(D(k))_{ab} = \sigma_0 \delta_{ab} + \begin{pmatrix} + & & & \\ & - & & \\ & & - & \\ & & & + \end{pmatrix} i\pi_0 + i \begin{pmatrix} & & & + \\ & & + & \\ & - & & \\ - & & & \end{pmatrix} \cos\frac{k_1}{2} \cos\frac{k_2}{2} + \begin{pmatrix} 0 & i\sin\frac{k_1}{2} & i\sin\frac{k_2}{2} & 0 \\ i\sin\frac{k_1}{2} & 0 & 0 & -i\sin\frac{k_2}{2} \\ i\sin\frac{k_2}{2} & 0 & 0 & i\sin\frac{k_1}{2} \\ 0 & -i\sin\frac{k_2}{2} & i\sin\frac{k_1}{2} & 0 \end{pmatrix}. \tag{34}$$

Then $\det D$ is given by

$$\begin{aligned} \det(D(k))_{ab} &= (\sigma_0^2 + \pi_0^2 + s^2)^2 - 2c_1^2 c_2^2 (\sigma_0^2 - \pi_0^2 - s^2) + c_1^4 c_2^4 \\ &= ((\sigma_0 + c_1 c_2)^2 + \pi_0^2 + s^2)((\sigma_0 - c_1 c_2)^2 + \pi_0^2 + s^2), \end{aligned} \tag{35}$$

where $s_\mu = \sin k_\mu/2$, $s^2 = \sum_\mu s_\mu^2$, $c_\mu = \cos k_\mu/2$. It is notable that this determinant is expressed by the product of the two determinants of the naive fermions with the flavored mass $\pm M_f^{(1)}(k_\mu/2)$. Now we can explicitly write the saddle-point conditions satisfied by σ_0 and π_0 as

$$\frac{\sigma_0 - M}{g^2} = 4 \int \frac{dk^2}{(2\pi)^2} \frac{\sigma_0(\sigma_0^2 + \pi_0^2 + s^2) - c_1^2 c_2^2 \sigma_0}{((\sigma_0 + c_1 c_2)^2 + \pi_0^2 + s^2)((\sigma_0 - c_1 c_2)^2 + \pi_0^2 + s^2)}, \tag{36}$$

$$\frac{\pi_0}{g^2} = 4 \int \frac{dk^2}{(2\pi)^2} \frac{\pi_0(\sigma_0^2 + \pi_0^2 + s^2) + c_1^2 c_2^2 \pi_0}{((\sigma_0 + c_1 c_2)^2 + \pi_0^2 + s^2)((\sigma_0 - c_1 c_2)^2 + \pi_0^2 + s^2)}. \tag{37}$$

By multiplying -1 to the first equation, we see $(-\sigma_0, \pi_0)$ are solutions for $(-M, g^2)$ if (σ_0, π_0) are solutions for (M, g^2). It also means, if (M_c, g^2) is a critical point, $(-M_c, g^2)$ too. The phase diagram will be symmetric about $M = 0$. The parity-phase boundary $M_c(g^2)$ in this case is derived by imposing $\pi_0 = 0$ in (36) and (37) after the overall π_0 being removed in the second one. Then the gap equations are given by

$$\frac{M_c}{g^2} = 4 \int \frac{dk^2}{(2\pi)^2} \frac{2c_1^2 c_2^2 \sigma_0}{((\sigma_0 + c_1 c_2)^2 + \pi_0^2 + s^2)((\sigma_0 - c_1 c_2)^2 + \pi_0^2 + s^2)}, \tag{38}$$

$$\frac{1}{g^2} = 4 \int \frac{dk^2}{(2\pi)^2} \frac{\sigma_0^2 + s^2 + c_1^2 c_2^2}{((\sigma_0 + c_1 c_2)^2 + \pi_0^2 + s^2)((\sigma_0 - c_1 c_2)^2 + \pi_0^2 + s^2)}. \tag{39}$$

By removing σ_0 in these equations, we derive the phase boundary $M_c(g^2)$. The result is shown in Fig. 4.

Here again A stands for the parity-symmetric phase ($\pi_0 = 0$) and B for Aoki phase ($\pi_0 \neq 0$). In the large coupling region there are two phase boundaries while there are four phase boundaries in the weak coupling region. The left cusp corresponds to one of two tastes with $m = 1$, and the right corresponds to the other taste with $m = -1$. Thus the phase diagram reflects the mass splitting of tastes given by the Adams-type flavored mass. We also check the pion mass becomes zero on the second-order phase boundary as

$$m_\pi^2 \propto \left\langle \frac{\delta^2 S_{\rm eff}}{\delta\pi_n \delta\pi_m} \right\rangle \Big|_{M=M_c} = V \frac{\delta^2 \tilde{S}_{\rm eff}}{\delta^2 \pi_0^2} \Big|_{M=M_c} = 0. \tag{40}$$

Now let us consider the parity-phase structure in the $d = 4$ QCD with the staggered fermion with this flavored mass. Considering the case of the Wilson fermion we can speculate it is qualitatively similar to our result for the $d = 2$ Gross-Neveu model except the number of species associated with each cusp. In the four dimension, four tastes in the staggered fermion with the Adams-type flavored mass split into two with positive mass and the other two with

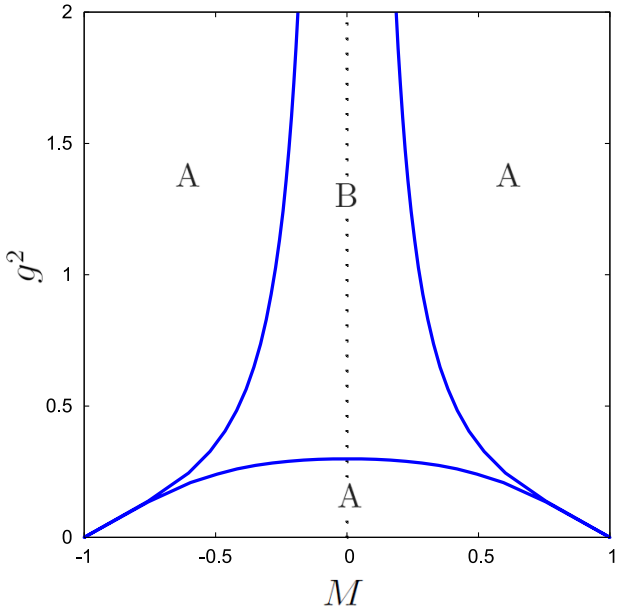

FIG. 4 (color online). Aoki phase structure for the staggered fermion with the Adams-type flavored mass $\Gamma_5\Gamma_{55}$. The left and right cusps correspond to one of two tastes with $m = 1$ and the other with $m = -1$. A stands for a parity-symmetric phase and B for Aoki phase.

negative mass depending on their flavor chiralities. Thus each of the cusps in the phase diagram will correspond to two tastes. If we consider another type of the flavored mass term proposed in [19], the four tastes are split into one with positive mass, two with zero mass and the other with negative mass. If we can take the chiral and continuum limit around the cusps, we obtain the two- or one-flavor staggered fermions with tuning only the mass parameter, which will be numerically faster than Wilson fermion. Thus the question here is whether we can take the massless continuum limit. We will discuss this point in the next section with starting with the case of the naive fermion.

IV. CONTINUUM LIMIT

In this section we discuss the continuum limit of the naive and staggered Gross-Neveu models with the flavored masses discussed in Secs. II and III. This analysis gives us important informations on the continuum limit of the $d = 4$ QCD with these fermions. As is well known, the chiral symmetry is realized in the effective potential of the Gross-Neveu model as the $O(2)$ rotational symmetry about σ_0 and π_0. The purpose here is to figure out the fine-tuned values of the mass and couplings to recover this symmetry for $a \to 0$. We note in order to take the chiral and continuum limit in this model, we need to introduce two independent couplings g_σ^2 and g_π^2 [3] as we will see later. The strategy is to expand the fermion determinant in the effective potential with respect to the lattice spacing a following the process in [3].

We first consider the case of the naive fermion with one of the flavored masses $M_f^{(1)} = \cos k_1 \cos k_2$. The effective potential in this case with the lattice spacing being explicit is given by

$$\tilde{S}_{\text{eff}}(\sigma_0, \pi_0) = \frac{(\sigma_0 - M)^2}{2g_\sigma^2} + \frac{\pi_0^2}{2g_\pi^2} - I, \tag{41}$$

$$I = \int_{-\pi/a}^{\pi/a} \frac{d^2k}{(2\pi)^2} \log\Big[\Big(\sigma_0 + \frac{1}{a}\cos k_1 a \cos k_2 a\Big)^2 + \pi_0^2 + \sum_\mu \frac{\sin^2 k_\mu a}{a^2}\Big]. \tag{42}$$

Now we divide the terms in the determinant I into $\mathcal{O}(1/a^2)$ and $\mathcal{O}(1/a)$ parts as

$$I(D_0, D_1) = \int_{-\pi/a}^{\pi/a} \frac{d^2k}{(2\pi)^2} \log[D_0 + D_1], \tag{43}$$

$$D_0 \equiv \sum_\mu \frac{\sin^2 k_\mu a}{a^2} + \Big(\sigma_0 - \frac{\alpha}{a}\Big)^2 + \pi_0^2 + \Big(\frac{\alpha + \cos k_1 a \cos k_2 a}{a}\Big)^2. \tag{44}$$

$$D_1 \equiv 2\Big(\sigma_0 - \frac{\alpha}{a}\Big)\Big(\frac{\alpha + \cos k_1 a \cos k_2 a}{a}\Big), \tag{45}$$

where we introduce a constant α since there is arbitrariness about how to divide the terms into $\mathcal{O}(1/a^2)$ and $\mathcal{O}(1/a)$ parts. This is determined by which cusp you choose in Fig. 1, or equivalently which species you want to make massless in the continuum limit. Here we fix $\alpha = -1$ which is related to the left cusp or the continuum limit with the massless species $(0, 0)$ and (π, π). (With $\alpha = 1$ we can discuss the other cusp while we will discuss $\alpha = 0$ in the end of this section.) Here we use the shifted definition of σ_0 as $\sigma_0 + 1/a \to \sigma_0$ for simplicity for a while. Then the effective potential with this shift is given by

$$\tilde{S}_{\text{eff}}(\sigma_0, \pi_0) = \frac{(\sigma_0 - (M + 1/a))^2}{2g_\sigma^2} + \frac{\pi_0^2}{2g_\pi^2} - I(D_0, D_1). \tag{46}$$

$$D_0 = \sum_\mu \frac{\sin^2 k_\mu a}{a^2} + \sigma_0^2 + \pi_0^2 + \Big(\frac{-1 + \cos k_1 a \cos k_2 a}{a}\Big)^2. \tag{47}$$

$$D_1 = 2\sigma_0\Big(\frac{-1 + \cos k_1 a \cos k_2 a}{a}\Big). \tag{48}$$

We expand I by D_1/D_0 or equivalently by the lattice spacing a,

$$I = I_0 + \sum_{n=1} I_n, \tag{49}$$

$$I_0 = \int_{-\pi/a}^{\pi/a} \frac{d^2k}{(2\pi)^2} \log D_0, \tag{50}$$

$$\begin{aligned} I_n &= -\frac{(-1)^n}{n} \int_{-\pi/a}^{\pi/a} \frac{d^2k}{(2\pi)^2} \frac{D_1^n}{D_0^n} \quad (n \geq 1), \\ &= -\frac{(-1)^n}{n} (2\sigma_0)^n a^{n-2} \times \int_{-\pi}^{\pi} \frac{d^2\xi}{(2\pi)^2} \\ &\quad \times \frac{(-1 + \cos\xi_1 \cos\xi_2)^n}{\left(\sum_\mu \sin^2\xi_\mu + (-1 + \cos\xi_1 \cos\xi_2)^2 + a^2(\sigma_0^2 + \pi_0^2) \right)^n}, \end{aligned} \tag{51}$$

where we introduce the dimensionless momentum $\xi_\mu = k_\mu a$. For $a \to 0$, only the I_0, I_1 and I_2 remains nonzero. $I_0(a \to 0)$, $I_1(a \to 0)$ and $I_2(a \to 0)$ are given by

$$\begin{aligned} I_0(a \to 0) &= \tilde{C}_0(\sigma_0^2 + \pi_0^2) - \frac{1}{2\pi}(\sigma_0^2 + \pi_0^2) \\ &\quad \times \log \frac{a^2(\sigma_0^2 + \pi_0^2)}{e} \quad (\tilde{C}_0 = 0.367), \end{aligned} \tag{52}$$

$$I_1(a \to 0) = \frac{2\sigma_0}{a} C_1 \qquad (C_1 = -0.446), \tag{53}$$

$$I_2(a \to 0) = -2\sigma_0^2 C_2 \qquad (C_2 = 0.201). \tag{54}$$

From here we basically do not care about the $\mathcal{O}(a)$ corrections. Here we show the explicit values of $\tilde{C}_0$, C_1 and C_2 since they will be essential for the discussion later. The details of the calculations are shown in Appendix A 1. Now let us discuss the continuum limit of this theory. Including all the nonzero contributions for $a \to 0$, the effective potential is given by

$$\begin{aligned} \tilde{S}_{\text{eff}} &= -\left(\frac{M + 1/a}{g_\sigma^2} + \frac{2}{a} C_1 \right) \sigma_0 \\ &\quad + \left(\frac{1}{2g_\pi^2} - \tilde{C}_0 + \frac{1}{2\pi} \log a^2 \right) \pi_0^2 \\ &\quad + \left(\frac{1}{2g_\sigma^2} - \tilde{C}_0 + 2C_2 + \frac{1}{2\pi} \log a^2 \right) \sigma_0^2 \\ &\quad + \frac{1}{2\pi}(\sigma_0^2 + \pi_0^2) \log \frac{\sigma_0^2 + \pi_0^2}{e}. \end{aligned} \tag{55}$$

This indicates we need two independent couplings g_σ^2, g_π^2 to recover the $O(2)$ symmetry toward the continuum limit. In addition, getting rid of the σ_0 linear term leads to the massless limit. Then the natural fine-tuned parameters for the chirally symmetric continuum limit without $\mathcal{O}(a)$ corrections are given by

$$M = -\frac{2g_\sigma^2}{a} C_1 - 1, \tag{56}$$

$$g_\pi^2 = \frac{g_\sigma^2}{4C_2 g_\sigma^2 + 1}, \tag{57}$$

where Eq. (56) is obtained by imposing the coefficient of σ_0 and Eq. (57) is given by imposing the coefficients of σ_0^2 and π_0^2 coincide. To consider a renormalized theory with the chiral symmetry we introduce the scale parameter (Λ parameter) as

$$\Lambda a = \exp\left[\pi\tilde{C}_0 - 2\pi C_2 - \frac{\pi}{2g_\sigma^2} \right]. \tag{58}$$

With the natural fine-tuning (57), this definition of Λ leads to the coupling renormalization including a given by

$$\frac{1}{2g_\sigma^2} = \tilde{C}_0 - 2C_2 + \frac{1}{2\pi} \log\left(\frac{1}{\Lambda^2 a^2} \right), \tag{59}$$

$$\frac{1}{2g_\pi^2} = \tilde{C}_0 + \frac{1}{2\pi} \log\left(\frac{1}{\Lambda^2 a^2} \right). \tag{60}$$

Here we need to keep Λ finite when we take the continuum limit $a \to 0$. Then the renormalized effective potential with the chiral symmetry in the continuum limit is given by

$$\tilde{S}_{\text{eff}} = \frac{1}{2\pi}(\sigma_0^2 + \pi_0^2) \log \frac{\sigma_0^2 + \pi_0^2}{e\Lambda^2}. \tag{61}$$

We note the fine-tuned point $(M(g_\sigma^2), g_\pi^2(g_\sigma^2))$ in (56) and (57) specifies the line along which the continuum limit should be taken. At the minimum of this potential σ_0 has a nonzero value, which corresponds to the spontaneous chiral symmetry breaking.

Let us look at these fine-tuned parameters in terms of the phase diagram. By this we can verify our fine-tuning yields the chiral-symmetric continuum theory. We first consider the nonzero value of g_σ^2 as $g_\sigma^2 = 0.6$ to reveal properties of the phase diagram. By hiding the lattice parameter with $a = 1$ the fine-tuned point $(M(0.6), g_\pi^2(0.6))$ is given by

$$M(g_\sigma^2 = 0.6) = -0.464, \tag{62}$$

$$g_\pi^2(g_\sigma^2 = 0.6) = 0.404. \tag{63}$$

Now we consider the M-g_π^2 phase diagram with $g_\sigma^2 = 0.6$. According to the case of the Wilson Gross-Neveu model [6], the phase boundary has a self-crossing point and the fine-tuned point is located slightly inside and below the self-crossing point in the parity-symmetric phase. Besides the phase boundary naively derived from the gap equations no longer describes the true one near the self-crossing point, and we need study the effective potential to find the true critical lines including the first-order ones. Here we will show these situations are common with our cases. The gap equations for the two couplings are given by

$$M_c = \sigma_0\left(1 - \frac{g_\sigma^2}{g_\pi^2}\right) - 2g_\sigma^2 \int \frac{d^2k}{(2\pi)^2} \frac{M_f^{(1)}(k)}{(\sigma_0 + M_f^{(1)}(k))^2 + s^2}, \tag{64}$$

$$\frac{1}{g_\pi^2} = 2\int \frac{d^2k}{(2\pi)^2} \frac{1}{(\sigma_0 + M_f^{(1)}(k))^2 + s^2}. \tag{65}$$

Here we come back to the unshifted definition of σ_0. In Figs. 5 and 6 we depict the $M_c(g_\pi^2)$ phase boundary derived from the gap Eqs. (64) and (65) for $g_\sigma^2 = 0.6$. The latter is an expanded one near the self-crossing point with the true phase boundaries. In the both figures a cross point stands for the fine-tuned point without $\mathcal{O}(a)$ corrections (62) and (63). It is located slightly to the right and below the s elf-crossing point near the second-order phase boundary. We note this region is the parity-unbroken phase. The qualitative properties of this phase diagram remain toward $g_\sigma^2 \to 0$ where the whole structure moves down to $g_\pi^2 = 0$ with the first-order boundaries disappearing. Here the fine-tuned point (56) and (57) gets close to the endpoint of the second-order phase boundary at $(M, g_\pi^2) \to (-1, 0)$, which corresponds to two species $(0, 0)(\pi, \pi)$. Thus the continuum limit along this fine-tuned point yields the theory with chiral symmetry and two massless fermions, which leads to massless pions as Goldstone bosons.

Now we discuss the first order phase transition. Although it is not essential for our purpose because in the limit $g_\sigma^2 \to 0$ the first-order phase boundary disappears and the entire phase boundary becomes of second order, we can reveal other aspects of our fermions by investigating it. As shown in [6] there are two kinds of the first-order phase boundaries in the case of Wilson fermion. One is the parity-phase boundary, across which π_0 at the minimum of the effective potential changes from zero to nonzero. The other is related to σ_0, across which the sign of σ_0 at the minimum of the potential changes discontinuously. Now we will show both of them exist also in our case. We numerically calculate the effective potential in Eq. (42) and search the minimum of the potential. In Fig. 6 we depict the appearance of the first-order phase boundaries. Here we note the true parity-phase boundary of second order as a blue solid line coincides with the naively derived phase boundary as a blue dotted line at the both sides of the self-crossing. Then the second-order one coming from the left converts to the first order at some point, which is spilled out from the naively derived boundary. It ends at the point encountering the naively derived one again. The first-order phase boundary for σ_0 starts from this point, going down straight, and ends at $g_\pi^2 = 0$. In Fig. 7 we depict the order parameter π_0 as a function of M for some fixed values of g_π^2 around which the order changes in Fig. 6. Here we verify the order of the transition changes from the second to the first about the point. In Fig. 8 we depict the σ_0 potential for several values of M crossing the σ_0 phase boundary. (Here we can take $\pi_0 = 0$ since it is the parity-symmetric phase.) The value of σ_0 at the minimum changes from $\sigma_0 > -1$ to $\sigma_0 < -1$ in a form of the

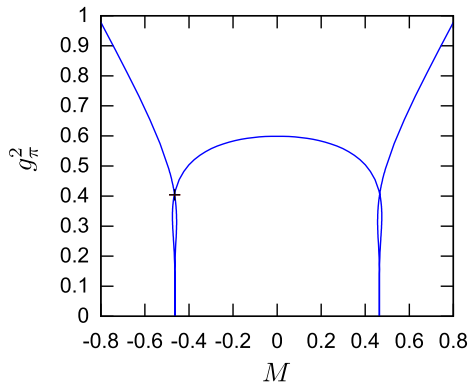

FIG. 5 (color online). The naively derived phase boundary $M(g_\pi^2)$ for the naive fermion with $M_f^{(1)}$ with $g_\sigma^2 = 0.6$. The fine-tuned point $(-0.464, 0.404)$ as a cross point is located near the self-crossing point.

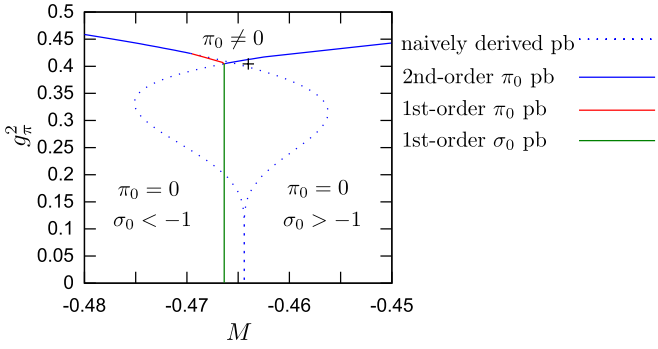

FIG. 6 (color online). An expanded version of Fig. 5. A blue dotted curve is the naively derived phase boundary. The true phase boundaries are composed of the three parts. The fine-tuned point as a cross point is located slightly to the right and below the self-crossing point.

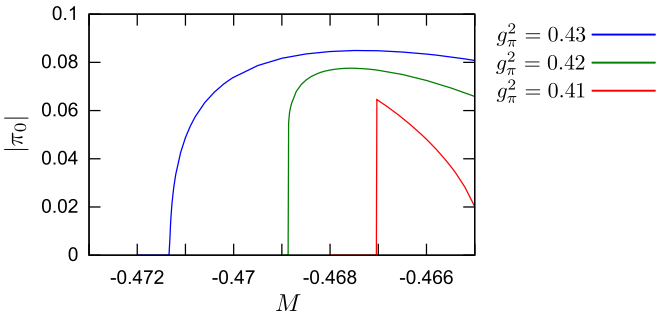

FIG. 7 (color online). The order parameter π_0 as a function of M for $g_\pi^2 = 0.41, 0.42, 0.43$ where the order of transition changes from first to second in Fig. 6.

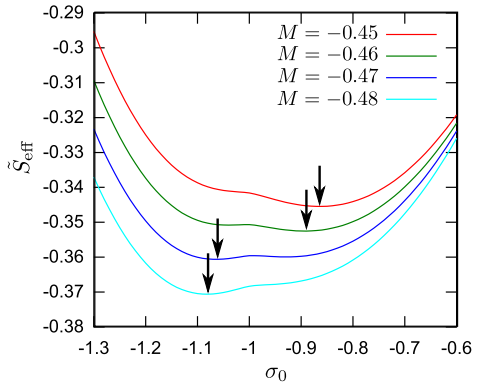

FIG. 8 (color online). The σ_0 potential for several values of M crossing the σ_0 boundary in Fig. 6. The value of σ_0 at the minimum changes from $\sigma_0 > -1$ to $\sigma_0 < -1$ in a form of the first-order transition.

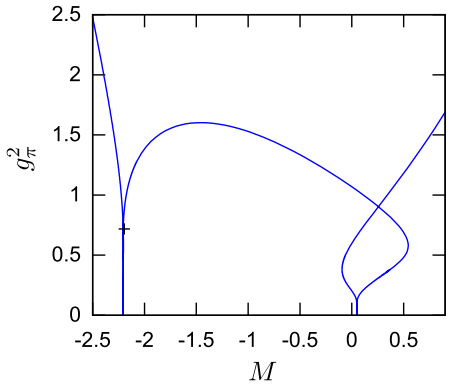

FIG. 9 (color online). The naively derived phase boundary $M_c(g_\pi^2)$ in the case of the naive fermion with $M_f^{(1)} + M_f^{(2)}$ for $g_\sigma^2 = 1.2$. The fine-tuned point $(-2.205, 0.720)$ as a cross point is located near the self-crossing point.

first-order phase transition. Indeed the potential describing these first-order transitions is also obtained by taking account of $\mathcal{O}(a)$ corrections. The contribution from the correction $\delta\tilde{S}_{\rm eff}$ is given by

$$\delta\tilde{S}_{\rm eff} = -\frac{8}{3}C_3\sigma_0^3 + 2\sigma_0(\sigma_0^2 + \pi_0^2) \times\left(\tilde{C}_1 + \frac{1}{4\pi}\log\frac{\sigma_0^2 + \pi_0^2}{e}\right), \tag{66}$$

with $C_3 = -0.0923$ and $\tilde{C}_1 = -0.0741$. We can qualitatively reproduce the above results from the effective potential with these corrections. We can obtain the same but reversed phase structure for the right cusp by choosing $\alpha = 1/a$ in (44) and (45). We also note the sign of σ_0 continuously changes at $M = 0$. It is related with the discrete chiral symmetry ($\sigma_0 \to -\sigma_0$) of the effective action (42) for $M = 0$ up to a irrelevant sign. This symmetry indicates interesting possibility of another continuum limit corresponding to the case of $\alpha = 0$ in (44) and (45). We will discuss details on this topic in the end of this section.

In Figs. 9 and 10 we depict the corresponding figures for the flavored mass $M_f^{(1)} + M_f^{(2)}$. We take $g_\sigma^2 = 1.2$ to make the structure enhanced, where the fine-tuned point for the left cusp is given by $(M, g_\pi^2) = (-2.205, 0.720)$. The results are qualitatively the same as the previous case. In this case the continuum limit along with the fine-tuned point leads to the single-flavor theory with one of the species at (0, 0).

We apply the same approach to the staggered Gross-Neveu model with the Adams-type flavored mass in Eq. (25). As seen in Eq. (35), the determinant in the logarithm in the effective action is given by the product of two determinants of the naive fermions with the mass $\pm M_f = \pm\cos(k_1/2)\cos(k_2/2)$. Thus we only have to add the contributions from the two sectors. Here we take the constant α as $\alpha = -1/a$ and redefine $\sigma_0 + 1/a \to \sigma_0$ for a while. With this choice we can discuss the left cusp related to the taste with the positive flavor chirality. Then the effective potential with the σ_0 shift is given by

$$\tilde{S}_{\rm eff}(\sigma_0, \pi_0) = \frac{(\sigma_0 - (M + 1/a))^2}{2g_\sigma^2} + \frac{\pi_0^2}{2g_\pi^2} - I^+ - I^-, \tag{67}$$

$$I^\pm = \int_{-\pi/a}^{\pi/a}\frac{d^2k}{(2\pi)^2}\log[D_0^\pm + D_1^\pm], \tag{68}$$

$$D_0^\pm = \sum_\mu \frac{\sin^2\frac{k_\mu a}{2}}{a^2} + \sigma_0^2 + \pi_0^2 + \left(\frac{-1 \pm \cos\frac{k_1 a}{2}\cos\frac{k_2 a}{2}}{a}\right)^2. \tag{69}$$

$$D_1^\pm = 2\sigma_0\left(\frac{-1 \pm \cos\frac{k_1 a}{2}\cos\frac{k_2 a}{2}}{a}\right). \tag{70}$$

We expand I with respect to D_1/D_0 as

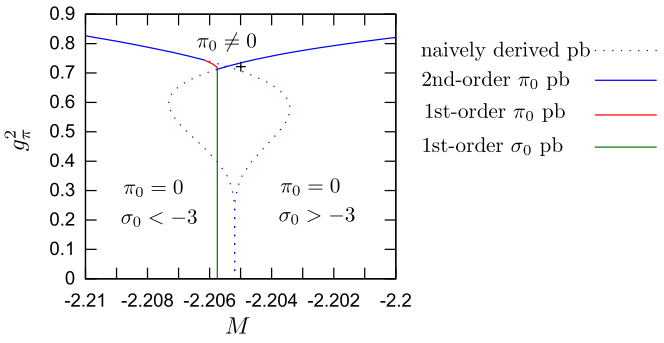

FIG. 10 (color online). An expanded version of Fig. 9. A blue dotted curve is the naively derived phase boundary. The true phase boundaries are composed of the three parts. The fine-tuned point is located slightly to the right and below the self-crossing point.

$$I^{\pm} = I_0^{\pm} + \sum_{n=1} I_n^{\pm}, \tag{71}$$

$$I_0^{\pm} = \int_{-\pi/a}^{\pi/a} \frac{d^2k}{(2\pi)^2} \log D_0^{\pm}, \tag{72}$$

$$I_n^{\pm} = -\frac{(-1)^n}{n} \int_{-\pi/a}^{\pi/a} \frac{d^2k}{(2\pi)^2} \frac{(D_1^{\pm})^n}{(D_0^{\pm})^n} \qquad (n \geq 1), \tag{73}$$

For the continuum limit $a \to 0$, only the $I_0^{\pm}$, $I_1^{\pm}$ and $I_2^{\pm}$ remains nonzero as in the previous case.

$$I_0^+ + I_0^- = \tilde{C}_0(\sigma_0^2 + \pi_0^2) - \frac{1}{\pi}(\sigma_0^2 + \pi_0^2) \times \log \frac{4a^2(\sigma_0^2 + \pi_0^2)}{e} \quad (\tilde{C}_0 = 1.177), \tag{74}$$

$$I_1^+ + I_1^- = \frac{2\sigma_0}{a} C_1 \qquad (C_1 = -0.896), \tag{75}$$

$$I_2^+ + I_2^- = -2\sigma_0^2 C_2 \qquad (C_2 = 0.404). \tag{76}$$

Details of calculations are shown in Appendix A 2. The effective potential and the fine-tuned point without $\mathcal{O}(a)$ corrections $(M(g_\sigma^2), g_\pi^2(g_\sigma^2))$ are given by the equations similar to Eqs. (55)–(61) as following. The effective potential for $a \to 0$ in this case is given by

$$\begin{aligned} \tilde{S}_{\text{eff}} = &-\left(\frac{M + 1/a}{g_\sigma^2} + \frac{2}{a} C_1\right)\sigma_0 \\ &+ \left(\frac{1}{2g_\pi^2} - \tilde{C}_0 + \frac{1}{\pi} \log 4a^2\right)\pi_0^2 \\ &+ \left(\frac{1}{2g_\sigma^2} - \tilde{C}_0 + 2C_2 + \frac{1}{\pi} \log 4a^2\right)\sigma_0^2 \\ &+ \frac{1}{\pi}(\sigma_0^2 + \pi_0^2) \log \frac{\sigma_0^2 + \pi_0^2}{e}. \end{aligned} \tag{77}$$

Then the tuned point for the chiral limit without $\mathcal{O}(a)$ corrections is

$$M = -\frac{2g_\sigma^2}{a} C_1 - 1, \tag{78}$$

$$g_\pi^2 = \frac{g_\sigma^2}{4C_2 g_\sigma^2 + 1}, \tag{79}$$

We again introduce the scale parameter (Λ-parameter) as

$$2a\Lambda = \exp\left[\frac{\pi}{2}\tilde{C}_0 - \pi C_2 - \frac{\pi}{4g_\sigma^2}\right]. \tag{80}$$

where we note the lattice spacing a always appears with a factor 2, which is specific to the staggered fermions. The coupling renormalization for the chiral and continuum limit is given by

$$\frac{1}{2g_\sigma^2} = \tilde{C}_0 - 2C_2 + \frac{1}{\pi} \log\left(\frac{1}{4\Lambda^2 a^2}\right), \tag{81}$$

$$\frac{1}{2g_\pi^2} = \tilde{C}_0 + \frac{1}{\pi} \log\left(\frac{1}{4\Lambda^2 a^2}\right), \tag{82}$$

where we keep Λ finite when taking the continuum limit $a \to 0$. Finally the renormalized effective potential in the chiral and continuum limit is given by

$$\tilde{S}_{\text{eff}} = \frac{1}{\pi}(\sigma_0^2 + \pi_0^2) \log \frac{\sigma_0^2 + \pi_0^2}{e\Lambda^2}. \tag{83}$$

In this case we take $g_\sigma^2 = 0.4$ as an example, then the fine-tuned point is given by

$$M(g_\sigma^2 = 0.4) = -0.286, \tag{84}$$

$$g_\pi^2(g_\sigma^2 = 0.4) = 0.243. \tag{85}$$

The gap equations in this case are given by

$$M_c = \sigma_0\left(1 - \frac{g_\sigma^2}{g_\pi^2}\right) + 8g_\sigma^2\sigma_0 \int \frac{dk^2}{(2\pi)^2} \times \frac{c_1^2 c_2^2}{((\sigma_0 + c_1c_2)^2 + \pi_0^2 + s^2)((\sigma_0 - c_1c_2)^2 + \pi_0^2 + s^2)}, \tag{86}$$

$$\frac{1}{g_\pi^2} = 4 \int \frac{dk^2}{(2\pi)^2} \times \frac{\sigma_0^2 + s^2 + c_1^2 c_2^2}{((\sigma_0 + c_1c_2)^2 + \pi_0^2 + s^2)((\sigma_0 - c_1c_2)^2 + \pi_0^2 + s^2)}. \tag{87}$$

Here we come back to the unshifted definition of σ_0. In Figs. 11 and 12 we depict the phase boundary $M(g_\pi^2)$ naively derived from the above gap equations for $g_\sigma^2 = 0.4$. The latter is an expanded one near the

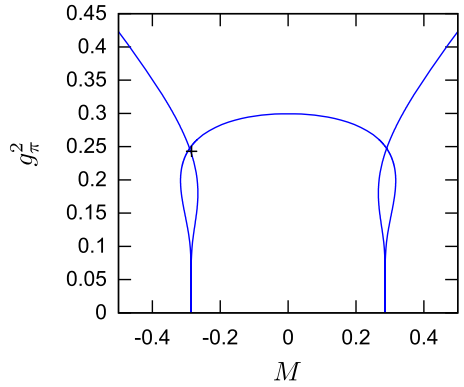

FIG. 11 (color online). The naively derived phase boundary $M_c(g_\pi^2)$ for the staggered fermion with the Adams-type mass with $g_\sigma^2 = 0.4$. The fine-tuned point $(-0.286, 0.243)$ as a cross point is located near the self-crossing point.

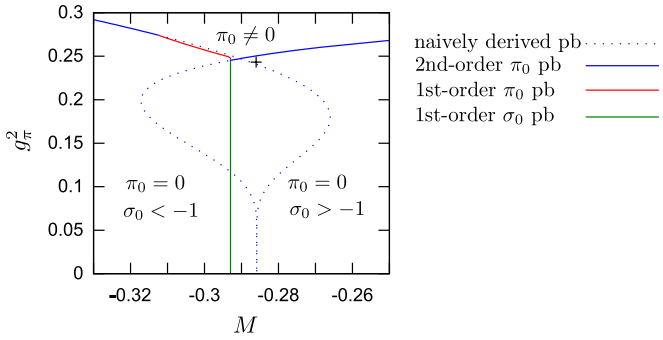

FIG. 12 (color online). The expanded version of Fig. 11. A blue dotted curve is the naively derived phase boundary. The true phase boundaries are composed of the three parts. The fine-tuned point is located slightly to the right and below the self-crossing point.

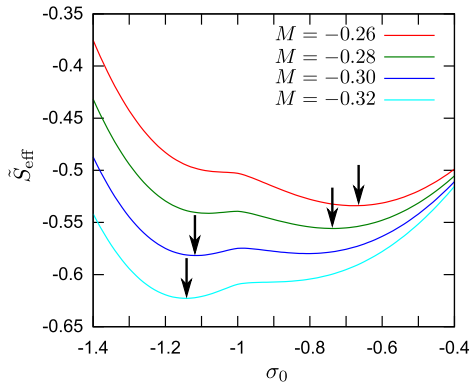

FIG. 14 (color online). The σ_0 potential for several values of M crossing the σ_0 boundary in Fig. 12. The value of σ_0 at the minimum changes from $\sigma_0 > -1$ to $\sigma_0 < -1$ in a form of the first-order transition.

self-crossing point with the true phase boundaries also depicted. The fine-tuned point (84) and (85) is located slightly to the right and below the self-crossing point near the true second-order phase boundary in the parity-symmetric phase. Toward the weak-coupling limit $g_\sigma^2 \to 0$ the phase structure moves down to $g_\pi^2 = 0$, where the fine-tuned point gets close to $(M, g_\pi^2) \to (-1, 0)$ from the parity-symmetric phase. It means our fine-tuned point leads to the continuum theory with the chiral symmetry and one massless fermion corresponding to the taste with positive flavor chirality. The situation about the first order phase boundary is the same as the naive case. In Fig. 12 we depict the true phase boundaries for this case. In Fig. 13 we depict the order parameter π_0 as a function of M. Here the order of the transition changes from the second to the first around the order-changing point. In Fig. 14 we depict the σ_0 potential for several values of M crossing the σ_0 phase boundary. The value of σ_0 at the minimum changes from $\sigma_0 > -1$ to $\sigma_0 < -1$ in a form of the first-order phase transition.

We have shown that the chirally-symmetric continuum limit can be taken by fine-tuning a mass parameter and two-coupling constants both for the naive and staggered

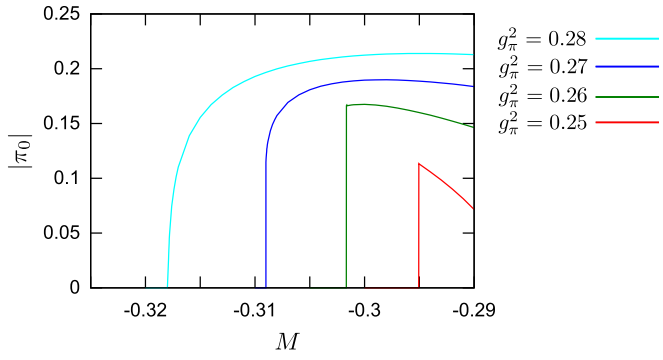

FIG. 13 (color online). The order parameter π_0 as a function of M for $g_\pi^2 = 0.25, 0.26, 0.27, 0.28$ where the order of transition changes from first to second in Fig. 12.

cases. It indicates we obtain the two-flavor or one-flavor massless fermions in the chiral limit by tuning only a mass parameter when we introduce the Adams-type [18] or Hoelbling-type [19] flavored masses to the $d = 4$ QCD with staggered fermions. We speculate the process to take the chiral and continuum limit could be almost the same as the case for Wilson fermion while the numerical cost will be less for the staggered fermions. The less numerical expense in the staggered fermion could make the QCD simulations with these fermions faster than Wilson fermion. We need further investigation to answer this question.

Now we comment on the case that we take $\alpha = 0$ in (44) and (45), which corresponds to neither of the cusps but reflects the symmetries of the effective potential. At this point the coupling is not going to zero, and thus it is unclear how it is related to the continuum Gross-Neveu model. However it does seem to be possible to restore chiral symmetry there and have a divergent correlation length. As such it seems related to a quite special continuum limit. Since the $M = 0$ effective potentials for the naive with $M_f^{(1)}$ and the staggered fermions with the Adams-type mass possess the Z_2 discrete chiral symmetry ($\sigma_0 \to -\sigma_0$) up to a irrelevant sign, the renormalization in the linear σ_0 term is prohibited. Actually we have checked C_1 in the effective potentials as (55) is zero for both cases with $\alpha = 0$. This is because the continuum chiral symmetry is broken while the discrete one is unbroken by these flavored masses. Thus, if we start with $M = 0$, it appears we need not fine-tune the mass parameter for the massless continuum limit with the chiral symmetry. It indicates a strange possibility that the chirally symmetric continuum limit of the $d = 4$ QCD with these fermions is taken without fine-tuning due to this symmetry. This strange situation can occur for any flavored mass with the discrete chiral symmetry up to a trivial sign such as $M_f = \sum_\mu \cos k_\mu$. However the question is whether the continuum limit

stands for physically relevant theories. Indeed it is unlikely since the line $M = 0$ is located at the same distance from the two cusps thus the continuum limit along it would have no physical fermions, although there might exist some relevant theory without fermions like the Ising theory. On the other hand, in the naive fermion with $M_f^{(2)}$ or the $d = 4$ staggered fermion with the mass proposed by Hoelbling in [19], the $M = 0$ line has a cusp in the weak coupling region. The effective actions in these cases also have the discrete chiral symmetry and the same situation occurs. Thus, the continuum limit without fine-tuning in them may lead to the relevant theories with the parity symmetry being broken since the continuum limit is taken from the Aoki phase in these cases. This kind of the parity or CP broken theory with massless fermions would belong to the same universality class as minimally doubled fermions [23,24] or the two-flavor QCD with the sign of mass being different between the two flavors [31]. Further study on this topic is devoted to the future work.

V. SUMMARY AND DISCUSSION

In this paper we investigate the parity-broken phase structure for naive and staggered fermions with the flavored mass by using the two-dimensional lattice Gross-Neveu models. We have shown the Aoki phase exists both in staggered and naive cases reflecting the mass splitting in species.

In Sec. II we study the phase structure for the naive Gross-Neveu model with the flavored masses. We consider the two types of flavored mass terms for two-dimensional naive fermions, which cause two different kinds of mass splitting in species. We also consider a linear combination of these terms. We solve the gap equations for the large N limit and obtain the second-order phase boundaries in the M-g^2 plane. The parity-broken phase diagram has some common properties with the Wilson case, and reflects the mass splitting. We can make varieties of phase structures depending on arbitrary linear combinations of the two types of the masses. In Sec. III we consider the generalized staggered Gross-Neveu model including two types of four-point interactions. We take the same process as in the case of the naive fermion to obtain the phase diagram for the staggered fermion with the Adams-type flavored mass. We show the Aoki phase exists also in this case reflecting the mass splitting of tastes. This elucidation can contribute to the practical application of these fermions and their overlap versions. In Sec. IV we discuss the continuum limit of these Gross-Neveu models around the cusps in the phase digram. We show that the chirally symmetric continuum limit with the number of massless species associated with each of the cusps can be taken by fine-tuning a mass parameter and two-coupling constants in both cases. From this we speculate the chiral limit can be taken by fine-tuning only a mass parameter in $d = 4$ lattice QCD with staggered fermions with the Adams-type [18] or Hoelbling-type [19] masses. It indicates we can obtain the one- or two-flavor massless fermions in the continuum from the staggered setup and regard massless pions as Goldstone bosons due to the spontaneous chiral symmetry breaking as in the case with Wilson fermion. These approaches avoid the use of the rooting approximation to reduce the number of tastes. We also study the first order phase boundaries peculiar to the two-coupling cases of the lattice Gross-Neveu models. We show there exist two kinds of the first order phase boundaries with respect to parity and chiral symmetry breaking as in the case of Wilson fermion.

We comment on the possible advances of the one-flavor or two-flavor staggered fermions without rooting discussed in this paper compared to Wilson fermion. Taking account of less numerical expense in the staggered fermion, it will be numerically better than Wilson fermion in the lattice QCD simulations. We can estimate how good it is easily by calculating simple examples. Future works will be devoted to this study.

ACKNOWLEDGMENTS

M. C. is grateful to the Alexander von Humboldt Foundation for support for visits to the University of Mainz. This manuscript has been authored under contract number DE-AC02-98CH10886 with the U.S. Department of Energy. Accordingly, the U.S. Government retains a nonexclusive, royalty-free license to publish or reproduce the published form of this contribution, or allow others to do so, for U.S. Government purposes. T. K. is supported by the JSPS Institutional Program for Young Researcher Overseas Visits. T. M. is grateful to Taku Izubuchi for fruitful discussion and hearty encouragement. T. M. is supported by Grand-in-Aid for the Japan Society for Promotion of Science (JSPS).

APPENDIX A: DERIVATION OF THE EFFECTIVE POTENTIALS

In this appendix we evaluate the integrals which are required for the effective potentials for the cases with the naive and staggered fermions.

1. Naive fermion

We have to evaluate the integrals of (50) and (51) to obtain the effective potential of the model with the naive fermion. Let us first study the following integral,

$$I_0 = \int_{-\pi/a}^{\pi/a} \frac{d^2k}{(2\pi)^2} \log\left[\frac{s^2}{a^2} + \sigma_0^2 + \pi_0^2 + \left(\frac{-1 + M_f}{a}\right)^2\right], \tag{A1}$$

where we denote $s^2 = \sum_\mu \sin^2(k_\mu a)$ and $M_f = \cos(k_1 a) \times \cos(k_2 a)$. If we omit a constant term which is not involving σ_0 and π_0, it can be rewritten in an integral representation as

$$I_0 \simeq \int_0^{\sigma_0^2+\pi_0^2} d\rho F_0(\rho), \tag{A2}$$

$$F_0(\rho) = \int_{-\pi/a}^{\pi/a} \frac{d^2k}{(2\pi)^2} \frac{1}{s^2/a^2 + (-1+M_f)^2/a^2 + \rho}. \tag{A3}$$

We pick up the divergent part in the limit of $a \to 0$,

$$F_0(\rho) \overset{a\to 0}{\to} \int_{-\pi/(2a)}^{3\pi/(2a)} \frac{d^2k}{(2\pi)^2} \times \left(\frac{1}{\sum_\mu k_\mu^2 + \rho} + \frac{1}{\sum_\mu (k_\mu - \pi)^2 + \rho} \right) + c_0, \tag{A4}$$

$$c_0 = \int_{-\pi/2}^{3\pi/2} \frac{d^2\xi}{(2\pi)^2} \left(\frac{1}{s^2 + (-1+M_f)^2} - \frac{1}{\sum_\mu \xi_\mu^2} - \frac{1}{\sum_\mu (\xi_\mu - \pi)^2} \right) \quad (= 0.0421). \tag{A5}$$

Here we shift the Brillouin zone to treat the divergent part, which originates from two massless modes around $k = (0, 0)$ and (π, π). We then find the following expression by comparing the first term with the corresponding integral in the continuum theory,

$$\int_{-\pi/(2a)}^{3\pi/(2a)} \frac{d^2k}{(2\pi)^2} \left(\frac{1}{\sum_\mu k_\mu^2 + \rho} + \frac{1}{\sum_\mu (k_\mu - \pi)^2 + \rho} \right) = \frac{1}{2\pi} \log \frac{1}{a^2\rho} + c_0' \qquad (c_0' = 0.325). \tag{A6}$$

Therefore the integral is given by

$$F_0(\rho) = \frac{1}{2\pi} \log \frac{1}{a^2\rho} + \tilde{C}_0 \qquad (\tilde{C}_0 = 0.367), \tag{A7}$$

where $\tilde{C}_0 = c_0 + c_0'$ is the constant used in (52). By substituting this into (A2), we obtain the expression in (52)

$$I_0(a \to 0) = \tilde{C}(\sigma_0^2 + \pi_0^2) - \frac{1}{2\pi}(\sigma_0^2 + \pi_0^2) \log \frac{a^2(\sigma_0^2 + \pi_0^2)}{e}. \tag{A8}$$

Next we show the integral expressions of (53) and (54). They are given by

$$C_1 = \int_{-\pi}^{\pi} \frac{d^2\xi}{(2\pi)^2} \frac{-1+M_f}{s^2 + (-1+M_f)^2} \quad (= -0.446), \tag{A9}$$

$$C_2 = \int_{-\pi}^{\pi} \frac{d^2\xi}{(2\pi)^2} \left(\frac{-1+M_f}{s^2 + (-1+M_f)^2} \right)^2 \quad (= 0.201). \tag{A10}$$

These integrals are sufficient to consider the continuum limit of the model, but not to discuss the first-order phase transition. The $\mathcal{O}(a)$ corrections come from the following integrals:

$$I_3(a \to 0) = \frac{8}{3}\sigma_0^3 a C_3,$$
$$C_3 = \int_{-\pi}^{\pi} \frac{d^2\xi}{(2\pi)^2} \left(\frac{-1+M_f}{s^2 + (-1+M_f)^2} \right)^3 \quad (= -0.0923), \tag{A11}$$

$$\delta I_1 = I_1 - \frac{2\sigma_0}{a} C_1 = 2\sigma_0 \int_{-\pi/a}^{\pi/a} \frac{d^2k}{(2\pi)^2} \left(\frac{(-1+M_f)/a}{s^2/a^2 + (-1+M_f)^2/a^2 + \sigma_0^2 + \pi_0^2} - \frac{(-1+M_f)/a}{s^2/a^2 + (-1+M_f)^2/a^2} \right) = -2\sigma_0 a \int_0^{\sigma_0^2+\pi_0^2} d\rho F_1(\rho), \tag{A12}$$

$$F_1(\rho) = \frac{1}{a} \int_{-\pi/a}^{\pi/a} \frac{d^2k}{(2\pi)^2} \frac{(-1+M_f)/a}{(s^2/a^2 + (-1+M_f)^2/a^2 + \rho)^2}. \tag{A13}$$

We can evaluate the second one in a similar way by splitting into a divergent part and a finite constant,

$$F_1(\rho) \overset{a\to 0}{\to} -\frac{1}{2} \int_{-\pi/(2a)}^{3\pi/(2a)} \frac{d^2k}{(2\pi)^2} \times \left(\frac{\sum_\mu k_\mu^2}{(\sum_\mu k_\mu^2 + \rho)^2} + \frac{\sum_\mu (k_\mu - \pi)^2}{(\sum_\mu (k_\mu - \pi)^2 + \rho)^2} \right) + c_1 \tag{A14}$$

$$c_1 = \int_{-\pi/2}^{3\pi/2} \frac{d^2\xi}{(2\pi)^2} \left(\frac{(-1+M_f)}{(s^2 + (-1+M_f)^2)^2} + \frac{1}{2\sum_\mu \xi_\mu^2} + \frac{1}{2\sum_\mu (\xi_\mu - \pi)^2} \right) \quad (= 0.00912). \tag{A15}$$

The divergent part is given by

$$\int_{-\pi/(2a)}^{3\pi/(2a)} \frac{d^2k}{(2\pi)^2} \left(\frac{\sum_\mu k_\mu^2}{(\sum_\mu k_\mu^2 + \rho)^2} + \frac{\sum_\mu (k_\mu - \pi)^2}{(\sum_\mu (k_\mu - \pi)^2 + \rho)^2} \right) = \frac{1}{2\pi} \log \frac{1}{a^2\rho} + c_1' \qquad (c_1' = 0.166). \tag{A16}$$

Thus we obtain

$$F_1(\rho) = -\frac{1}{4\pi} \log \frac{1}{a^2\rho} + \tilde{C}_1 \qquad \left(\tilde{C}_1 = c_1 - \frac{c_1'}{2} = -0.0741 \right). \tag{A17}$$

By substituting this expression into (A12), we obtain

$$\delta I_1 = -2\sigma_0 a\Big[\tilde{C}_1(\sigma_0^2+\pi_0^2) + \frac{1}{4\pi}(\sigma_0^2+\pi_0^2)\log\frac{a^2(\sigma_0^2+\pi_0^2)}{e}\Big]. \quad \text{(A18)}$$

These integrals contribute to the $\mathcal{O}(a)$ corrections to the effective potential (66).

2. Staggered fermion

We evaluate the integrals required for the effective potentials with the staggered fermion. Explicit forms of the finite constants in (75) and (76) are simply given by

$$C_1 = \int_{-\pi}^{\pi}\frac{d^2\xi}{(2\pi)^2}\Big[\frac{-1+M_f}{s^2+(-1+M_f)}+\frac{-1-M_f}{s^2+(-1-M_f)}\Big] \quad (=-0.896), \quad \text{(A19)}$$

$$C_2 = \int_{-\pi}^{\pi}\frac{d^2\xi}{(2\pi)^2}\Big[\Big(\frac{-1+M_f}{s^2+(-1+M_f)}\Big)^2 + \Big(\frac{-1-M_f}{s^2+(-1-M_f)}\Big)^2\Big] \quad (=0.404), \quad \text{(A20)}$$

where we use similar symbols as the naive fermion case, $s^2=\sum_\mu \sin^2(k_\mu a/2)$, $M_f=\cos(k_1 a/2)\cos(k_2 a/2)$.

The integral (74) is slightly complicated, but can be evaluated in a similar manner. Omitting a constant term independent on σ_0 and π_0, it can be written as

$$I_0^+ = \int_{-\pi/a}^{\pi/a}\frac{d^2k}{(2\pi)^2}\log\Big[\frac{s^2}{a^2}+\sigma_0^2+\pi_0^2+\Big(\frac{-1+M_f}{a}\Big)^2\Big] \simeq \int_0^{\sigma_0^2+\pi_0^2} d\rho F(\rho), \quad \text{(A21)}$$

$$F(\rho) = \int_{-\pi/a}^{\pi/a}\frac{d^2k}{(2\pi)^2}\frac{1}{s^2/a^2+(-1+M_f)^2/a^2+\rho}. \quad \text{(A22)}$$

We can split this integral into a divergent part and a finite constant in the limit of $a\to 0$,

$$F(\rho)\overset{a\to 0}{\to}\int_{-\pi/a}^{\pi/a}\frac{d^2k}{(2\pi)^2}\frac{1}{\sum_\mu k_\mu^2/4+\rho}+c_0^+,$$

$$c_0^+ = \int_{-\pi}^{\pi}\frac{d^2\xi}{(2\pi)^2}\Big(\frac{1}{s^2+(-1+M_f)^2}-\frac{1}{\sum_\mu \xi_\mu^2/4}\Big) \quad (=0.0440). \quad \text{(A23)}$$

The divergent part is given by

$$\int_{-\pi/a}^{\pi/a}\frac{d^2k}{(2\pi)^2}\frac{1}{\sum_\mu k_\mu^2/4+\rho} = \frac{1}{\pi}\log\frac{1}{4a^2\rho}+C_0^{+\prime} \qquad (C_0^{+\prime}=0.798). \quad \text{(A24)}$$

Thus we obtain

$$F(\rho) = \frac{1}{\pi}\log\frac{1}{4a^2\rho}+\tilde{C}_0^+ \qquad (\tilde{C}_0^+ = C_0^+ + C_0^{+\prime} = 0.842). \quad \text{(A25)}$$

The corresponding integral becomes

$$I_0^+(a\to 0) = \tilde{C}_0^+(\sigma_0^2+\pi_0^2) - \frac{1}{\pi}(\sigma_0^2+\pi_0^2)\log\frac{4a^2(\sigma_0^2+\pi_0^2)}{e}. \quad \text{(A26)}$$

The other integral is written as

$$I_0^- \simeq C_0^-(\sigma_0^2+\pi_0^2)+\mathcal{O}(a), \quad \text{(A27)}$$

$$C_0^- = \int_{-\pi}^{\pi}\frac{d^2\xi}{(2\pi)^2}\frac{1}{s^2+(1+M_f)^2} \quad (=0.333) \quad \text{(A28)}$$

where we again omit a constant independent on σ_0 and π_0. As a result we obtain the expression of (74),

$$I_0^+ + I_0^- = \tilde{C}_0(\sigma_0^2+\pi_0^2) - \frac{1}{\pi}(\sigma_0^2+\pi_0^2)\log\frac{4a^2(\sigma_0^2+\pi_0^2)}{e} \qquad (\tilde{C}_0 = \tilde{C}_0^+ + C_0^- = 1.177). \quad \text{(A29)}$$

[1] S. Aoki, Phys. Rev. D **30**, 2653 (1984).
[2] S. Aoki, Phys. Rev. D **33**, 2399 (1986); **34**, 3170 (1986); Phys. Rev. Lett. **57**, 3136 (1986); Nucl. Phys. **B314**, 79 (1989).
[3] S. Aoki and K. Higashijima, Prog. Theor. Phys. **76**, 521 (1986).
[4] M. Creutz, arXiv:hep-lat/9608024.
[5] S. Sharpe and R. Singleton, Jr., Phys. Rev. D **58**, 074501 (1998).
[6] T. Izubuchi, J. Noaki, and A. Ukawa, Phys. Rev. D **58**, 114507 (1998).
[7] K. G. Wilson, Phys. Rev. D **10**, 2445 (1974).
[8] H. B. Nielsen and M. Ninomiya, Nucl. Phys. **B185**, 20 (1981); **B193**, 173 (1981); Phys. Lett. **105B**, 219 (1981).

[9] P. H. Ginsparg and K. G. Wilson, Phys. Rev. D **25**, 2649 (1982).
[10] N. Neuberger, Phys. Lett. B **427**, 353 (1998).
[11] D. B. Kaplan, Phys. Lett. B **288**, 342 (1992).
[12] V. Furman and Y. Shamir, Nucl. Phys. **B439**, 54 (1995).
[13] T. Izubuchi and K. Nagai, Phys. Rev. D **61**, 094501 (2000).
[14] J. B. Kogut and L. Susskind, Phys. Rev. D **11**, 395 (1975).
[15] L. Susskind, Phys. Rev. D **16**, 3031 (1977).
[16] H. S. Sharatchandra, H. J. Thun, and P. Weisz, Nucl. Phys. **B192**, 205 (1981).
[17] D. H. Adams, Phys. Rev. Lett. **104**, 141602 (2010).
[18] D. H. Adams, arXiv:1008.2833.
[19] C. Hoelbling, Phys. Lett. B **696**, 422 (2011).
[20] M. Creutz, T. Kimura, and T. Misumi, J. High Energy Phys. 12 (2010) 041.
[21] L. H. Karsten, Phys. Lett. **104B**, 315 (1981).
[22] F. Wilczek, Phys. Rev. Lett. **59**, 2397 (1987).
[23] M. Creutz, J. High Energy Phys. 04 (2008) 017; A. Boriçi, Phys. Rev. D **78**, 074504 (2008).
[24] P. F. Bedaque, M. I. Buchoff, B. C. Tiburzi, and A. Walker-Loud, Phys. Lett. B **662**, 449 (2008); Phys. Rev. D **78**, 017502 (2008); S. Capitani, J. Weber, and H. Wittig, Phys. Lett. B **681**, 105 (2009); T. Kimura and T. Misumi, Prog. Theor. Phys. **124**, 415 (2010); **123**, 63 (2010); S. Capitani, M. Creutz, J. Weber, and H. Wittig, J. High Energy Phys. 09 (2010) 027; M. Creutz and T. Misumi, Phys. Rev. D **82**, 074502 (2010); T. Misumi, M. Creutz, and T. Kimura, Proc. Sci., LATTICE2010 (2010) 260.
[25] M. Creutz, Proc. Sci., LATTICE2010 (2010) 078.
[26] D. J. Gross and A. Neveu, Phys. Rev. D **10**, 3235 (1974).
[27] T. Eguchi and R. Nakayama, Phys. Lett. **126B**, 89 (1983).
[28] B. Leder, Ph.D. thesis, [arXiv:0707.1939].
[29] T. Korzec, Ph.D. thesis, http://edoc.hu-berlin.de/docviews/abstract.php?id=28045.
[30] B. Leder, J. High Energy Phys. 04 (2008) 044.
[31] M. Creutz, Phys. Rev. Lett. **92**, 201601 (2004); **92**, 162003 (2004).